ACS NANO

www.acsnano.org

# Redesigning Solvation Structure toward Passivation-Free Magnesium Metal Batteries

Juncai Long, Yi Liu, Ze He, Shuangshuang Tan, Fangyu Xiong, Hantao Xu, Weixiao Wang, Ge Zhang, Zhongzhuo Yang, and Qinyou An*

**Cite This:** *ACS Nano* 2024, 18, 15239−15248

Read Online

ACCESS | Metrics & More | Article Recommendations | Supporting Information

**ABSTRACT:** Simple magnesium (Mg) salt solutions are widely considered as promising electrolytes for next-generation rechargeable Mg metal batteries (RMBs) owing to the direct $Mg^{2+}$ storage mechanism. However, the passivation layer formed on Mg metal anodes in these electrolytes is considered the key challenge that limits its applicability. Numerous complex halogenide additives have been introduced to etch away the passivation layer, nevertheless, at the expense of the electrolyte's anodic stability and cathodes' cyclability. To overcome this dilemma, here, we design an electrolyte with a weakly coordinated solvation structure which enables passivation-free Mg deposition while maintaining a high anodic stability and cathodic compatibility. In detail, we successfully introduce a hexa-fluoroisopropyloxy ($HFIP^-$) anion into the solvation structure of $Mg^{2+}$, the weakly $[Mg-HFIP]^+$ contact ion pair facilitates $Mg^{2+}$ transportation across interfaces. As a consequence, our electrolyte shows outstanding compatibility with the RMBs. The Mg||PDI−EDA and Mg||$Mo_6S_8$ full cells use this electrolyte demonstrating a decent capacity retention of ∼80% over 400 cycles and 500 cycles, respectively. This represents a leap in cyclability over simple electrolytes in RMBs while the rest can barely cycle. This work offers an electrolyte system compatible with RMBs and brings deeper understanding of modifying the solvation structure toward practical electrolytes.

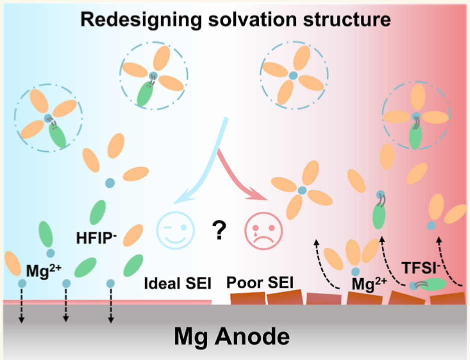

**KEYWORDS:** *magnesium metal batteries, electrolyte, passivation-free, solvation structure, solid electrolyte interface*

## 1. INTRODUCTION

The direct utilization of metal anodes is an attractive strategy to realize the high energy density of batteries. In striking contrast to the dendritic Li deposition behavior, Mg metal delivers smooth plating/stripping morphology during electrochemical cycles.[1] Owing to this dendrite-free merit as well as its high capacity (2205 mAh $g^{-1}$ and 3833 mAh $cm^{-3}$), affordability, and abundant resources of Mg metal, rechargeable Mg metal batteries (RMBs) are considered a promising candidate for future energy storage.[2] Nevertheless, the implementation of RMBs is plagued by a notorious passivation layer. Highly active Mg metal engages in reactions with most electrolyte components (including solvents, salts, and additives) to produce a dense passivation layer, which impedes any potential chemical reaction.[3] To mitigate the passivation layer obstruction in the Mg plating/stripping process, the predominant strategy over the past few decades has been using chlorine-containing electrolytes, whose corrosive components effectively etch away the passivation layer.[4−6] However, chlorine-containing electrolytes usually come at the expense of the electrolytes' oxidative stability and compatibility (cathode material and collector), which hinders high-voltage battery applications and deteriorates the battery performance.[7] Development of chlorine-free and passivation-free Mg electrolytes is imminent.[8]

Nevertheless, the prerequisites for building practical chlorine-free electrolytes are still unclear. Direct conversion of conventional Li salts into Mg salts as electrolytes for RMBs has proven unsuccessful, even in Mg-compatible ether solvents, distinct passivation can be observed in pure $Mg(TFSI)_2$ salt-based electrolytes.[9,10] However, some boron-based Mg salts with bulky delocalized anions [such as $Mg(BH_4)_2$,[11] $Mg(CB_{11}H_{12})_2$,[12] and $Mg[B(HFIP)_4]_2$[13] enable reversible Mg plating/stripping. These ambiguities hinder the precise design of passivation-free electrolyte systems. Recently, solvation engineering in chlorine-free simple salt electrolytes has led to several fascinating breakthroughs. Wang et al. designed a flexible solvation structure in $Mg(TFSI)_2$/1,2-dimethoxy-

**Received:** March 25, 2024
**Revised:** May 11, 2024
**Accepted:** May 22, 2024
**Published:** May 29, 2024

https://doi.org/10.1021/acsnano.4c03968

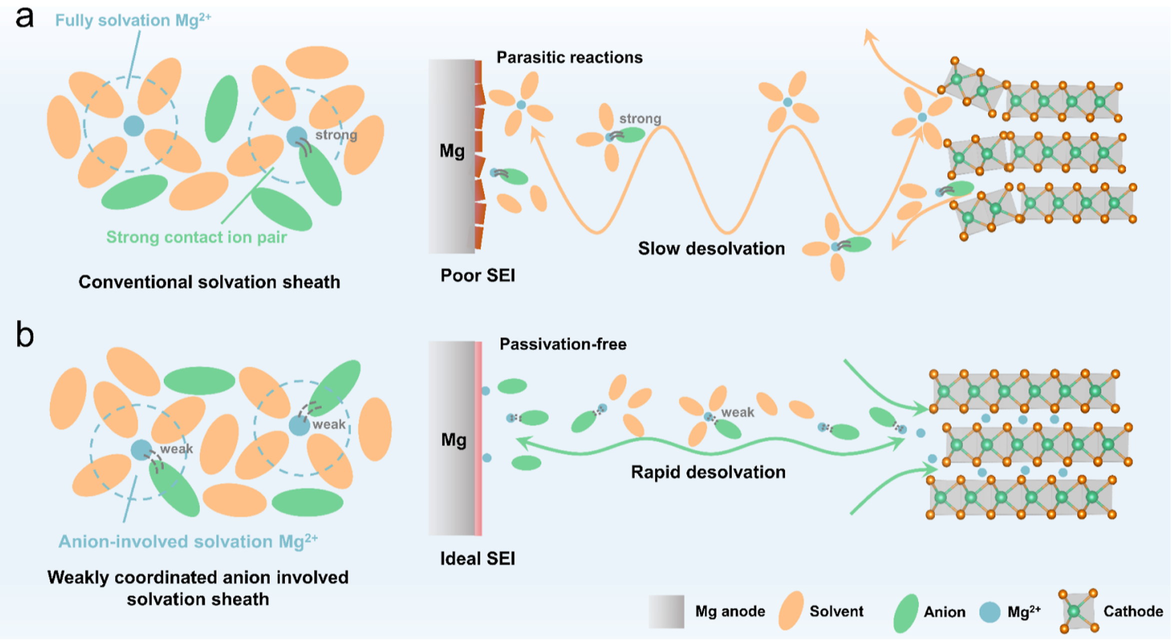

**Figure 1. Schematic illustrating the design concept for a weakly coordinated anion-involved solvation sheath. Solvation structure schematic and the process of $Mg^{2+}$ desolvation and intercalation in (a) conventional electrolyte and (b) weakly solvating electrolyte.**

ethane (DME) electrolyte for fast $Mg^{2+}$ (de) intercalation in high-voltage manganese oxides;[14] Yang et al. tuned $Mg^{2+}$ coordination structure with trimethyl phosphate additive enabling highly reversible Mg metal anodes;[15] Nuli and Tan et al. developed a methoxyethylamine cosolvent coordination $Mg(SO_3CF_3)_2$/ether electrolyte for optimized Mg plating/stripping.[16,17] Unfortunately, their implementation is also plagued by necessary additives and expensive costs. To date, apart from boron/aluminum-based Mg salts containing bulky delocalized anions, there is no simple Mg salt enabling efficient Mg plating/stripping with a single-solvent.

Inspired by the beneficial role of the solvation structure, herein, we present a solvation sheath with weakly coordinated anions that facilitates passivation-free Mg plating/stripping behavior. Via detailed molecular dynamics (MD) simulation and extensive spectroscopic studies, we identified that the more electron-localized fluoride alkyl Mg salts [$Mg(OCH(CF_3)_2)_2$, abbreviated as $Mg(HFIP)_2$; $Mg(OC(CF_3)_3)_2$, abbreviated as $Mg(PFTB)_2$] are more inclined to form weakly contact ion pair (CIP) structures in DME than the conventional $Mg(TFSI)_2$ salt. In this anion-enriched solvation environment, the charge density of $Mg^{2+}$ is diluted, thereby facilitating the desolvation process. Besides, rational regulation of the abundance of weakly CIPs and electrolyte concentration is also crucial. Among them, weakly solvating 2 M $Mg(HFIP)_2$ electrolyte demonstrate a higher Coulombic efficiency (CE, ~98.5%), decreased overpotential (150 mV), and improved oxidative stability (~3.5 V vs $Mg^{2+}$/Mg). Furthermore, multidimensional interfacial analysis reveals that this specialized solvation structure facilitates the formation of an anion−enrichment interface, which prevents the Mg metal anode from continuous passivation. Based on these improvements, $Mg(HFIP)_2$ electrolyte demonstrates excellent inorganic and organic cathode compatibility, contributing to the stable cycling of Mg metal full cells.

## 2. RESULTS AND DISCUSSION

The metal salt dissolves in the solvent, releasing anions and cations while acting as a medium, physically separating the two electrodes from direct electron transport and allowing working ions to be transported within the cell, which is the fundamental working mechanism of electrolyte.[18] In principle, any medium capable of conducting $Mg^{2+}$ may serve as the electrolyte; however, due to the extremely poor interfacial compatibility of the Mg anode, particular attention must be focused on the desolvation behavior at the electrode−electrolyte interface. Conventional chloride-free simple Mg-salt electrolytes [such as $Mg(TFSI)_2$, $Mg(CF_3SO_3)_2$, and $Mg(HMDS)_2$] typically form fully solvation $Mg^{2+}$ or strong CIPs, which have been proven to generate complex parasitic reactions on the anode that ultimately passivate the Mg metal and destroy the host structure on the cathode (Figure 1a).[15,19,20] Compared to monovalent metal ions, divalent $Mg^{2+}$ exhibit greater charge densities; reasonable designing solvation sheaths with weakly coordinated anions to mitigate cation−solvent interactions while ensuring rapid cation−anion dissociation could be a promising approach (Figure 1b).[21]

Previous work has already confirmed that fluoride alkyl ($HFIP^-$ and $PFTB^-$) can preferentially coordinate with $Mg^{2+}$ in chloride-containing electrolytes.[22] Besides, compared to the most typical $Mg(TFSI)_2$, the electron distribution of $Mg(HFIP)_2$ and $Mg(PFTB)_2$ is more centralized due to the smaller anionic structure (Figure S1), which is more favorable for the formation of CIPs. It is worth noting that these fluoride alkyl salts also have a high solubility in Mg-compatible ether solvents (Figure S2). Therefore, this beneficial structure is expected to be directly applicable to Mg electrolytes.

MD simulation was performed to provide a more intuitive comprehension of the difference between the solvation structure of these electrolytes with the conventional $Mg(TFSI)_2$ electrolyte. As expected, interactions between the $Mg^{2+}$−solvent (DME) and $Mg^{2+}$-anions exhibit contrasting trends. The $Mg^{2+}$ in $Mg(TFSI)_2$ electrolytes is strongly

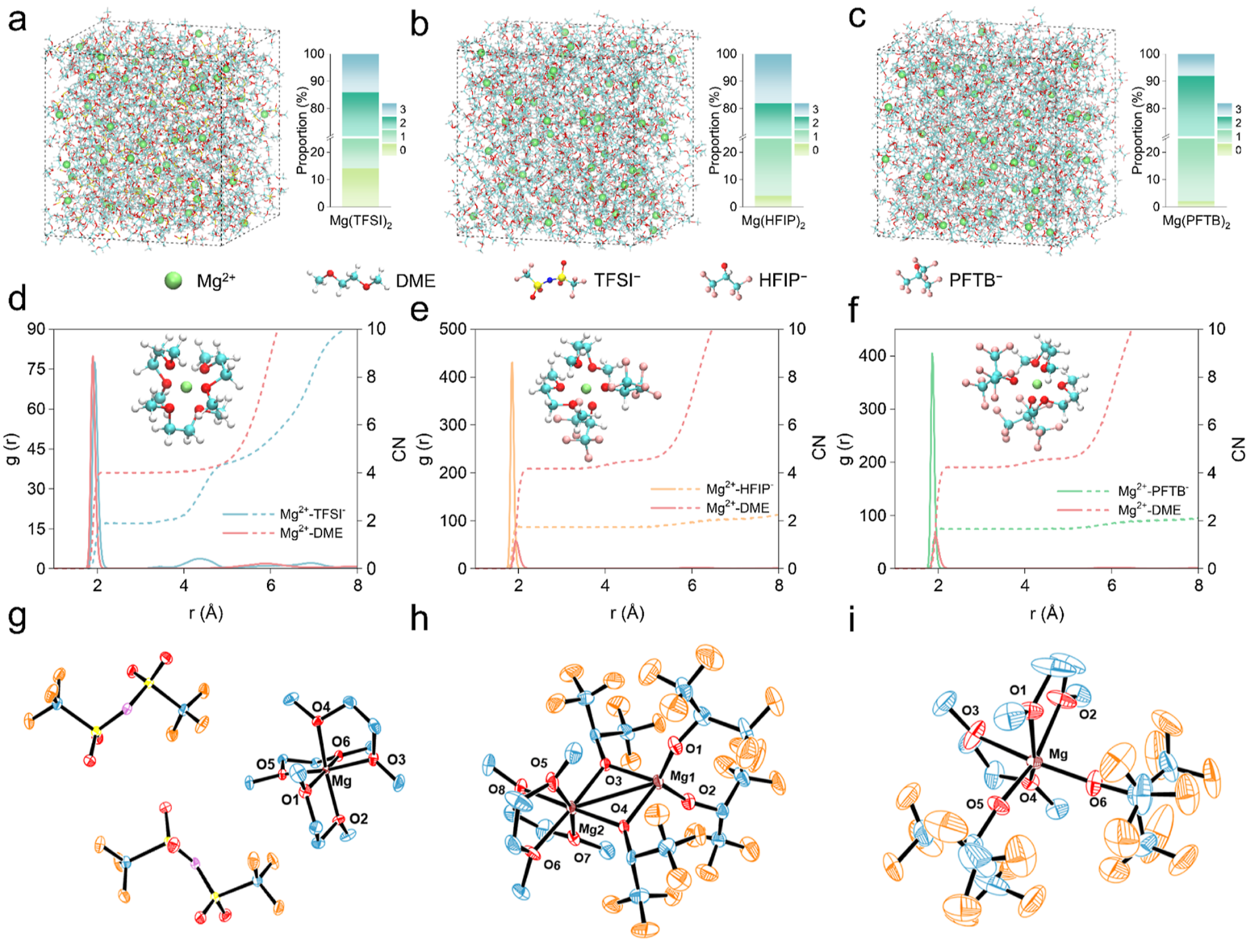

Figure 2. Simulation and characterization of solvation structures for different electrolytes. Snapshots of the MD simulation boxes and corresponding proportion distributions of solvation structures containing different numbers of anions for (a) Mg(TFSI)$_2$, (b) Mg(HFIP)$_2$, and (c) Mg(PFTB)$_2$ electrolytes. RDFs of interactions between Mg$^{2+}$ to solvent (DME), Mg$^{2+}$ to anions, and the coordination number of (d) Mg(TFSI)$_2$, (e) Mg(HFIP)$_2$, and (f) Mg(PFTB)$_2$ electrolytes. ORTEP plots of the coordination structure of crystallized (g) [Mg·3DME][2TFSI], (h) 2[Mg·2HFIP·DME], and (i) [Mg·2PFTB·DME], the thermal ellipsoid is shown at 40% probability. Yellow, S; red, O; orange, F; blue, C; brown, Mg; and purple, N.

coordinated with both anions and solvents. The simulated primary solvation sheath contains both solvent-separated ion pairs (SSIPs) and CIPs forms (Figure 2a), corresponding to the distinct radial distribution function (RDF) peaks (Figure 2d). The results of mass spectrometry were also consistent with the above description (Figure S3). On the other hand, Mg(HFIP)$_2$ and Mg(PFTB)$_2$ salts exhibit a reduced solvation effect that enables Mg$^{2+}$ to prior interact with the anion in the primary solvation shell, which is the classical CIPs and aggregate solvation structures (Figure 2b,c).[23] RDFs of these solvation structures are shown in Figure 2e,f, apparently, the $g(r)$ intensity of Mg$^{2+}$-anions is almost an order of magnitude greater than Mg$^{2+}$ to DME. The more electron-localized anions (HFIP$^-$ and PFTB$^-$) lead to competitive coordination between cations and anions; hence, the solvation sheath of Mg$^{2+}$ is always wrapped by anions. Additionally, the statistical proportions of the number of anions in the Mg$^{2+}$ solvation sheath in each electrolyte system are also consistent with the abovementioned results. In Mg(TFSI)$_2$ electrolytes, solvation structures without anionic participation are abundant, yet their proportion is almost 0% in Mg(HFIP)$_2$ and Mg(PFTB)$_2$ electrolytes. The snapshots of MD simulation present more visual evidence, in fully solvation Mg$^{2+}$(DME)$_3$, Mg$^{2+}$ is enclosed in a ring by three DME molecules in the Mg(TFSI)$_2$ electrolyte and forms a six-coordinated bridge with the oxygen atom in the DME, which has been confirmed by previous studies.[14,15] In contrast, Mg$^{2+}$ is surrounded by two DME molecules and two anions in an anion-involved solvation sheath in Mg(HFIP)$_2$ and Mg(PFTB)$_2$ electrolytes. Single-crystal X-ray diffraction of these three Mg salts in DME exhibited more convincing results. The minimum structural units in Mg(HFIP)$_2$ and Mg(PFTB)$_2$ electrolytes are 2[Mg·2HFIP·DME] (CCDC number: 2245741) and [Mg·2PFTB·DME] (CCDC number: 2245740),[22] respectively. However, in the Mg(TFSI)$_2$ electrolyte, Mg$^{2+}$ exhibits a greater tendency to coordinate with the solvent, resulting in the formation of [Mg·3DME][2TFSI] structure (Figure 2g–i and Table S1).[24]

Fourier transform infrared spectroscopy and nuclear magnetic resonance (NMR) measurements were carried out to distinguish the interaction between cations and solvent molecules experimentally. The C–O vibrations in DME near 1050 cm$^{-1}$ exhibited a blue shift in the Mg(TFSI)$_2$ electrolyte,

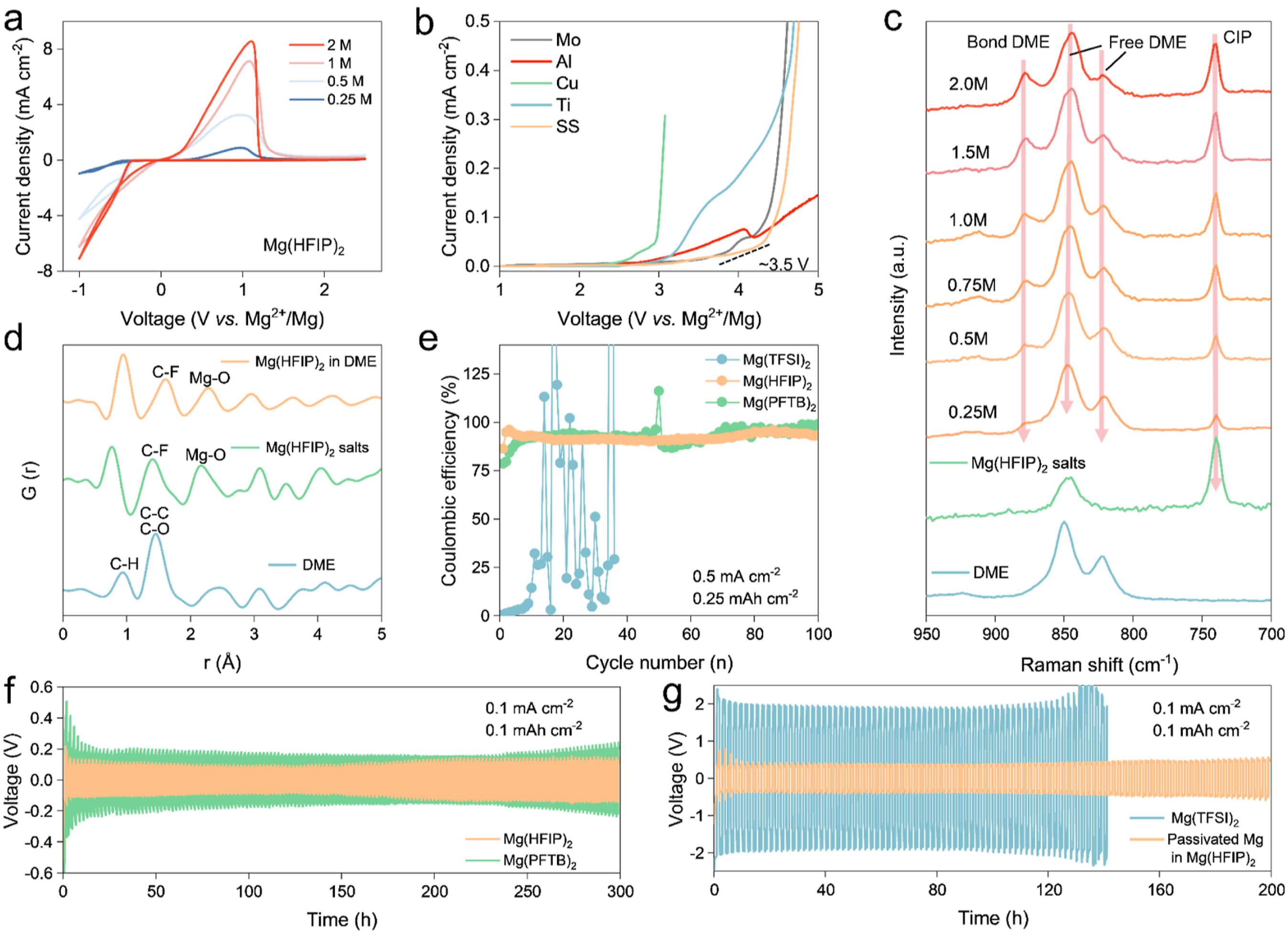

**Figure 3. Electrochemical and spectra analysis of electrolyte. (a) Cyclic voltammograms of the Mg plating/stripping process in various concentrations of the Mg(HFIP)$_2$ electrolyte at 25 mV s$^{-1}$. (b) Oxidation stability of 2 M Mg(HFIP)$_2$ electrolyte in different metal electrodes tested by linear sweep voltammetry. (c) Raman spectra of pure DME, Mg(HFIP)$_2$ salts, and Mg(HFIP)$_2$ electrolytes from 0.25 to 2 M. (d) PDFs of pure DME, Mg(HFIP)$_2$ salts, and 0.5 M Mg(HFIP)$_2$ electrolyte. (e) Mg plating/stripping CEs in Mg||SS asymmetric cells using different electrolytes at 0.5 mA cm$^{-2}$ and 0.25 mAh cm$^{-2}$. (f) Cycling performance of the Mg||Mg symmetric cells with Mg(HFIP)$_2$ and Mg(PFTB)$_2$ electrolytes at 0.1 mA cm$^{-2}$ and 0.1 mAh cm$^{-2}$. (g) Cycling performance of the Mg||Mg symmetric cells with Mg(TFSI)$_2$ (with polished Mg electrodes) and Mg(HFIP)$_2$ electrolytes (with passivated Mg electrodes) at 0.1 mA cm$^{-2}$ and 0.1 mAh cm$^{-2}$.**

which results from the inductive effect of electron-withdrawing Mg$^{2+}$.[25] In contrast, cation−solvent interactions in Mg(HFIP)$_2$ and Mg(PFTB)$_2$ electrolytes are drastically reduced in the presence of abundant CIPs (Figure S4). Besides, the NMR results of these electrolytes also exhibit the same tendency. The chemical shift of $^1$H signals in DME shows a red-shift in the order of Mg(TFSI)$_2$ > Mg(HFIP)$_2$ > Mg(PFTB)$_2$, which suggests that strong anion−solvent interactions lead to higher electron cloud densities, increased shielding effects, and reduced chemical shift values (Figure S5).[26] The $^{19}$F signals in anions also follow the same order, with increasing intimate interactions between anions and Mg$^{2+}$, the noticeable downfield (more positive) shift was observed (Figure S6). It is worth mentioning that in the Mg(TFSI)$_2$ electrolyte, strong Mg$^{2+}$(DME)$_3$ coordination structure leads to a pronounced downfield shift in the $^1$H signal of the part bonded DME molecule (4.1 and 4.4 ppm).[24] Nevertheless, even at elevated concentrations, no comparable shift was observed in the other electrolyte (Figure S7), confirming the more relaxed cation−solvent interaction.

In conclusion, both theoretical and experimental results suggest that an anion-involved solvation sheath shell is formed in the Mg(HFIP)$_2$ and Mg(PFTB)$_2$ electrolytes. This solvation structure holds the promise to reduce the charge density of Mg$^{2+}$ and weaken the cation−solvent interactions, leading to a rapid desolvation process at the electrode−electrolyte interface, and we will investigate this in more detail further on.

These simple Mg electrolytes were then subjected to preliminarily cyclic voltammetry tests using stainless-steel (SS) foil as the working electrode. As anticipated, Mg(HFIP)$_2$ and Mg(PFTB)$_2$ electrolytes both exhibit reversible plating/stripping curves (Figures 3a and S8), whereas blank Mg(TFSI)$_2$ electrolyte strongly passivate Mg metal anode (Figure S9).[27] Among the two weakly solvating electrolytes, the Mg(HFIP)$_2$ electrolyte exhibits improved plating/stripping efficiency and increased peak current at the elevated electrolyte concentration. That is probably due to a higher proportion of active weakly CIPs in high-concentration electrolytes, which can even be directly monitored by mass spectrometry (Figure S10). In addition, the decreased free DME proportion also contributes to the higher oxidative stability of the 2 M Mg(HFIP)$_2$ electrolyte, which reaches approximately 3.5 V in various nonprecious metal collectors (Figure 3b). Moreover, both conventional CE tests (Figure 3e) and standard Aurbach

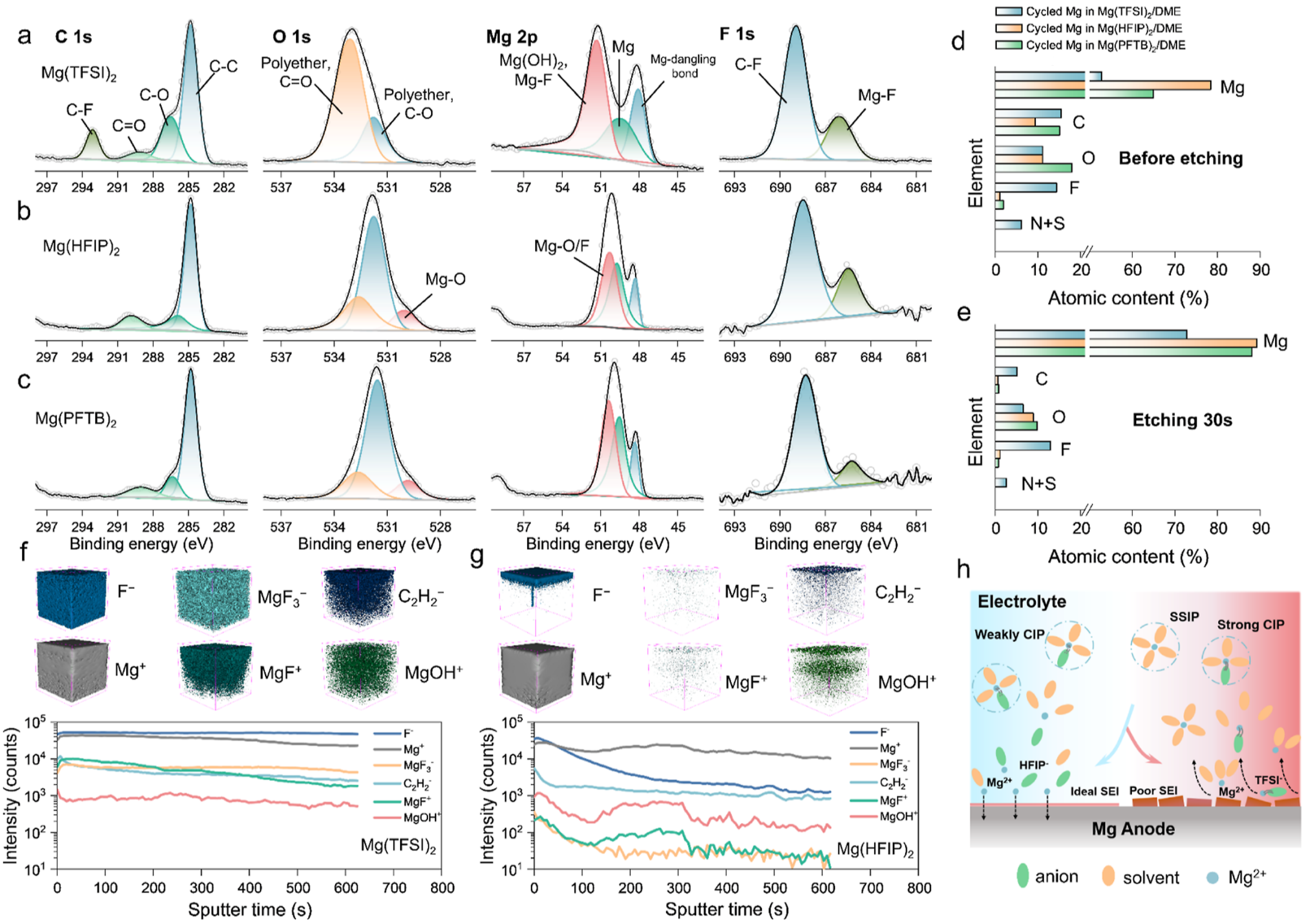

**Figure 4. Characterizations of the SEI layers on the Mg metal anodes. C 1s, O 1s, Mg 2p, and F 1s XPS spectra of the cycled Mg metal in (a) Mg(TFSI)$_2$, (b) Mg(HFIP)$_2$, and (c) Mg(PFTB)$_2$ electrolytes. Atomic contents of various elements (d) before and (e) after etching 30 s. TOF-SIMS 3D rendering models and depth profiles in the positive and negative modes of the SEI layers on the Mg metal anodes cycled in (f) Mg(TFSI)$_2$ and (g) Mg(HFIP)$_2$ electrolytes. (h) Illustrations of the desolvation process of conventional electrolytes (red zone) and weakly solvating electrolytes (blue zone) at Mg metal anodes.**

method tests (Figure S11) of this electrolyte show the average CE up to 98% in Mg||SS asymmetric cell.[28] In contrast, the absence of weakly CIPs results in the Mg(TFSI)$_2$ electrolyte, leading to direct passivation of the Mg metal anode, even when concentration is increased (Figure S12). Discrepancies of properties in weakly solvating electrolytes [Mg(HFIP)$_2$ and Mg(PFTB)$_2$] may also arise from differences in the content of active weakly solvating CIPs. The presence of three electron-withdrawing groups −CF$_3$ in the PFTB$^-$ anion facilitates dissociation from Mg$^{2+}$, resulting in a relatively low content of weakly CIPs, which hinders the effective Mg plating/stripping (Figures S13 and S14).[16] Furthermore, variations in the solvation structure result in significant discrepancies in the ionic conductivity of these electrolytes. The diffusion rate of cations in electrolytes is primarily influenced by the size of the solvated cations and the solvation structure. In the Mg(TFSI)$_2$ electrolyte, the abundance of more flexible SSIP solvation structures ensures the ultrahigh ionic conductivity through the vehicular shuttle mechanism. On the contrary, in weakly solvating electrolyte, cation shuttling occurs via slower structural transport modes, such as exchanging coordinating solvents with free solvents (Figure S15).[29] Considering the higher solubility and increased content of active weak CIPs, we selected 2 M Mg(HFIP)$_2$ electrolyte as the main research target for the following experiments.

Raman spectroscopy was employed to further investigate the effect of the electrolyte concentration on the solvation structures. The peak for solid salts, Mg(TFSI)$_2$ at 748 cm$^{-1}$ (Figure S16),[24] Mg(HFIP)$_2$ at 739 and 327 cm$^{-1}$ (Figures 3c and S17),[30] and Mg(PFTB)$_2$ at 762 cm$^{-1}$ (Figure S18), are typical for CIPs. However, upon dissolving salts in the solvent, the CIP peak exclusively persists in weakly solvating electrolytes, whereas a vibrational band at significantly lower wavenumbers is observed in the Mg(TFSI)$_2$ electrolyte, indicating the formation of SSIPs. Moreover, the existence of CIPs in the Mg(HFIP)$_2$ electrolyte even at an extreme salt: solvent molecular ratio (0.25 M) indicates the inherent incomplete dissociative nature of the salt.[31] Besides, pair distribution function (PDF) tests show that the local CIP organization of Mg salt molecules remains well-preserved in weakly solvating electrolytes, as evidenced by minor variations in the Mg−O bond lengths (Figures 3d and S19). However, the Mg−N bond in the Mg(TFSI)$_2$ salt nearly vanished after dissolution, corresponding to complete solvation of Mg$^{2+}$ (Figure S20).

Mg||Mg symmetric cells were assembled to assess the overall ion transport, particularly interfacial conduction. As expected,

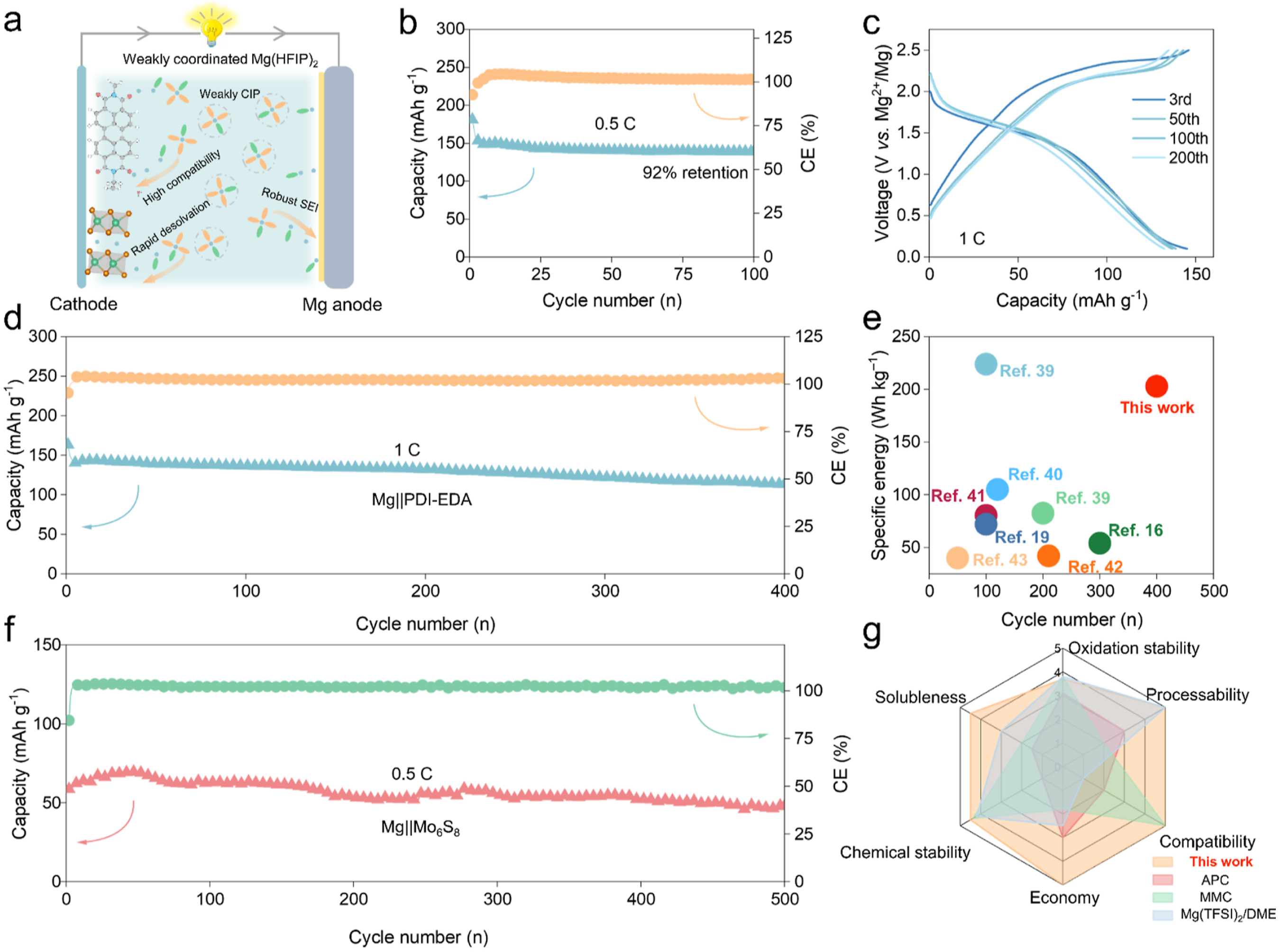

**Figure 5. Mg metal full cells tests. (a) Schematic illustrations of the working mechanism of the Mg(HFIP)$_2$ electrolyte. (b) Cycling performance of Mg||PDI−EDA full cell over 100 cycles at 0.5 C (1 C = 257 mAh g$^{-1}$). (c) Selected charge/discharge curves with a voltage range of 0.1−2.5 V (vs Mg$^{2+}$/Mg) and (d) long-term cycling performance at 1 C. (e) Performance comparison of Mg metal batteries that store Mg$^{2+}$ ions in simple Mg-salt electrolytes. The detailed calculation parameters are summarized in Table S2. (f) Long-term cycling performance of the Mg||Mo$_6$S$_8$ full cell at 0.5 C (1 C = 128 mAh g$^{-1}$). (g) Radar plots comparing this work to other reported representative electrolytes.**

Mg(HFIP)$_2$ and Mg(PFTB)$_2$ electrolytes demonstrated acceptable overpotentials at 0.1 mA cm$^{-2}$ (150 and 200 mV, respectively) (Figure 3f), and the Mg(HFIP)$_2$ electrolyte exhibits a low polarization (460 mV) even at 5 mA cm$^{-2}$ (Figure S21). In contrast, the Mg(TFSI)$_2$ electrolyte delivers a high overpotential exceeding 2 V. Previous studies have claimed that the passivation layer formed on the Mg anode leads to the unavailability of this electrolyte.[32,33] However, passivated Mg metal [after being cycled in the Mg(TFSI)$_2$ electrolyte] presents a low overpotential of 400 mV in the Mg(HFIP)$_2$ electrolyte and sustains a stable cycling for more than 200 h (Figure 3g). The passivation layer only slightly hinders the transportation of Mg$^{2+}$ at the interface in the Mg(HFIP)$_2$ electrolyte; obviously, the "passivation" of the Mg metal anode is more likely to be determined by the inherent solvation structure of the electrolyte.

To elucidate the desolvation mechanism of different solvation sheaths at the interface, our investigation further involved a comprehensive multidimensional characterization of the cycled Mg anode. Figure 4a−c displays the X-ray photoelectron spectroscopy (XPS) spectra of the Mg anode after cycling in Mg||Mg symmetric cells with different electrolytes. The results from C 1s and O 1s spectra suggest that the Mg anode cycled in the Mg(TFSI)$_2$ electrolyte has the highest signal intensity of C−F bond (293.2 eV)[34] and C═O bond (533 eV),[14] which is attributed to the extensive and incomplete decomposition of anions and solvents. Besides, crystalline Mg(OH)$_2$ (52 eV) and inorganic MgF$_2$ (685.2 eV) are also abundant on this passivation layer.[20] In contrast, reduced electrolyte residues and increased Mg metal signals (49.1 eV) were observed on the Mg anode cycled in weakly solvating electrolytes,[35] which implies the formation of a thinner anion-derived SEI layer. The detailed average elemental concentrations were further investigated via XPS etching. The sputter-depth profiles show organic species (C and O containing species) and fluorides (F element >10 at. %) accumulations on the Mg anode cycled in the Mg(TFSI)$_2$ electrolyte even after 30 s etching (Figure 4d,e). In contrast, following a brief etching period, there are almost no other impurities on the Mg anode cycled in Mg(HFIP)$_2$ and Mg(PFTB)$_2$ electrolytes (Mg element ~90 at. %), suggesting a significantly thinner SEI layer.

Time-of-flight secondary ion mass spectrometry (TOF-SIMS) was used to further assess the chemical state of these elements in SEI. As shown in the 3D reconstruction images in Figure 4f, the passivation layer in the $Mg(TFSI)_2$ electrolyte predominantly contains organic segments ($C_2H_2^-$) and fluorinated anionic fragments ($F^-$), besides, inorganic $MgF_3^-$, $MgF^+$, and $MgOH^+$ also abundantly present. During the $Mg^{2+}$ desolvation process, anions and organic ether-derived fragments accumulate and continuously react with the Mg anode (Figure S22), eventually forming a thick passivation layer. The $TFSI^-$ anion exhibits oxidative stability up to 4 V due to its relatively low highest occupied molecular orbital energy level, its comparatively low lowest unoccupied molecular orbital energy level results in its facile reduction and decomposition on the Mg metal anode (Figures S23 and S24). Therefore, the content of these species remains constant, even after 600 s sputtering. In contrast, Mg anode cycled in the $Mg(HFIP)_2$ electrolyte shows minimal quantities of organic fluorides and organic species adsorption (Figure 4g). In addition, this anion-derived SEI layer is present only on the very narrow surface of the Mg anode, again confirming a much thinner SEI layer formation that allows for rapid cross-interfacial transport of $Mg^{2+}$.

The solvation structure exerts a significant influence not only on the composition and thickness of the anode-electrolyte interface layer but also on the morphology of Mg metal deposition. Due to the lowest Mg plating/stripping overpotential, the deposited Mg in $Mg(PFTB)_2$ and $Mg(HFIP)_2$ electrolytes is more homogeneous,[36] and no corrosive craters are observed in the Mg metal anode after cycling (Figure S25).[37] In contrast, the intense desolvation process of $Mg^{2+}$ in the $Mg(TFSI)_2$ electrolyte leads to the formation of inhomogeneous black precipitates, and corresponding energy dispersive spectroscopy analysis shows that it is a mixture of deposited Mg and decomposed solvent (Figure S26). It is worth mentioning that all of the above test samples were prepared under an inert atmosphere; therefore, the results discussed in this work are excluded from the interference of air.

Based on a thorough analysis of the solvation structure and electrode−electrolyte interface, the passivation mechanism in simple Mg electrolytes is established (Figure 4h). In a conventional Mg solvation sheath, the divalent $Mg^{2+}$ with high charge density promotes the formation of SSIP and tight CIP structure. This interaction is strong and leads to increased overpotential during the desolvation process. As a result, the electrolyte components decompose, and a dense passivation layer is eventually formed on the Mg metal anode. In contrast, in weakly solvating electrolytes, the anion-involved solvation structure disperses the charge density of $Mg^{2+}$, thereby weakening its binding to the solvent and facilitating a rapid desolvation process. This solvation structure contributes to the formation of a thin anion-derived SEI layer, which enables the long-term stability of RMBs.

Given their excellent compatibility with Mg anodes and potential compatibility with cathodes due to their noncorrosive nature, $Mg(HFIP)_2$ and $Mg(PFTB)_2$ electrolytes were further evaluated in Mg metal full cells. The Mg||$Mo_6S_8$ full cell with the $Mg(PFTB)_2$ electrolyte exhibits a low reversible capacity of 52 mAh $g^{-1}$ at 0.2 C and experiences dramatic capacity fading within 40 cycles (Figure S27). This can be attributed to the low concentration of active weakly CIPs, which we have discussed abovementioned. On the contrary, in the $Mg(HFIP)_2$ electrolyte, the abundant easily dissociated [Mg−HFIP]$^+$ ion pairs facilitate a rapid desolvation process and simultaneously ensure the rapid diffusion of $Mg^{2+}$ in cathode materials. As a consequence, this chlorine-free $Mg(HFIP)_2$ electrolyte allows direct $Mg^{2+}$ storage in both organic and inorganic cathode (Figure 5a).[38] The Mg||PDI−EDA full cell delivers 90% capacity retention (141 mAh $g^{-1}$) after 100 cycles at 0.5 C (Figures 5b and S28). Besides, the cell was further tested at a higher current density of 1 C, which still realizes an 80% capacity retention (117 mAh $g^{-1}$) over 400 cycles. The corresponding charge−discharge profiles show a sloping plateau during the discharge process at an average of ∼1.4 V vs $Mg^{2+}$/Mg (Figure 5c,d). Such energy density and stability are at the forefront of simple Mg-salt electrolytes that store $Mg^{2+}$ (Figure 5e and Table S2).[16,19,39−43] We tested this electrolyte in different full cells to further assess its compatibility with a chalcogenide-based cathode and high-voltage Prussian blue analogue cathode. The Mg||$Mo_6S_8$ full cell with $Mg(HFIP)_2$ electrolyte demonstrates a reduced polarization, improved rate performance (Figures S29 and S30), and outstanding stable cycling at 0.5 C (Figure 5f). Besides, the typical Mg||CuS full cell and high-voltage Mg||FeHCF full battery also demonstrated reversible charge/discharge processes (Figures S31 and S32). To conclude, the properties of $Mg(HFIP)_2$ electrolyte are summarized in radar plots in Figure 5g, which exhibits a more comprehensively improved performance over other classical Mg electrolytes.[12,15,44]

## 3. CONCLUSIONS

In summary, we proposed an electrolyte that enables passivation-free Mg metal anode and reversible $Mg^{2+}$ ion storage in cathodes. By introducing an electron-localized fluoride alkyl Mg salt [$Mg(HFIP)_2$] in DME, we constructed a weakly coordinated anion-involved solvation sheath to mitigate the charge density of divalent $Mg^{2+}$. This beneficial solvation structure enables efficient Mg plating and stripping with single-salt and single-solvent. The as-designed electrolyte enables a highly reversible Mg anode and excellent compatibility with cathode materials. Moreover, our electrolyte features a low-cost, noncorrosive, highly compatible, and wide electrochemical window (∼3.5 V vs $Mg^{2+}$/Mg). As a result, the practical Mg metal full cells (with both organic and inorganic cathodes) using our electrolyte demonstrate an exceptional cycling stability. This work addresses the challenges of directly applying simple Mg-salt electrolytes in RMBs and brings insightful understanding toward the reasonable designing of organic multivalent ion electrolytes.

## 4. METHODS

**4.1. Electrolyte Preparation.** $Mg(TFSI)_2$ salt were purchased from Sigma-Aldrich. $Mg(HFIP)_2$ and $Mg(PFTB)_2$ salts were synthesized according to previous report.[22] Briefly, in an argon-filled glovebox, 1,1,1,3,3,3-hexafluoro-2-propanol [$(CF_3)_2CHOH$, 22 mmol] was dissolved in 10 mL of dry DME, then, 10 mL of di-*n*-butyl magnesium ([$CH_3(CH_2)_3]_2Mg$, 10 mmol, 1.0 M in heptane) solution was added slowly to the above solution and stirred overnight, the reaction is violently exothermic. Finally, the solvent is removed under vacuum to obtain a white powder, which is $Mg(HFIP)_2$ salt. $Mg(PFTB)_2$ salt were synthesized by the same procedure by regulating the 1,1,1,3,3,3-hexafluoro-2-propanol as perfluoro-*tert*-butyl alcohol [$(CF_3)_3COH$]. $Mg(HFIP)_2$ and $Mg(PFTB)_2$ salts must be vacuum-dried to remove traces of moisture. The electrolyte is easy to prepare, in an argon filled glovebox, different Mg salts are added separately to the DME solvent to form the transparent and stable solutions.

**4.2. Cathode Preparation.** *4.2.1. Synthesis of the $Mo_6S_8$ Cathode.* The Chevrel $Mo_6S_8$ was synthesized using a modified procedure to the previous work.[45] Briefly, 0.8 g of CuS, 1.6 g of $MoS_2$, 1.2 g of Mo powder, and 16 g of KCl were mixed and ball milled at 350 rpm for 3 h. The ground powder was then transferred to a crucible for sintering. Under a sealed argon atmosphere, the sample was sintered in a tubular furnace at 300 °C for 1 h, then, the sample was heated up to 1000 °C for another 24 h. After cooling to room temperature, the products were washed with deionized water, and $CuMo_6S_8$ could be obtained. As prepared, $CuMo_6S_8$ was then immersed into a 6 M HCl solution and stirred for 72 h. The solution was centrifuged, and $Mo_6S_8$ precipitates were washed with deionized water and dried under vacuum at 80 °C. The $Mo_6S_8$ cathodes were prepared by spreading the mixed slurry composed of 70 wt % $Mo_6S_8$ powder, 20 wt % super P, and 10 wt % polyvinylidene fluoride in the NMP solvent to SS foils and dried at 70 °C. The mass loading of the active material is about 1.5 mg $cm^{-2}$.

*4.2.2. Synthesis of the PDI−EDA Cathode.* PDI−EDA was synthesized using a modified procedure to the previous work.[46] Typically, perylene-3,4,9,10-tetracarboxylic dianhydride (0.5 mmol) and ethylenediamine (EDA) (0.5 mmol) were first dissolved in 50 mL of 1-methyl-2-pyrrolidinone (NMP). This procedure was carried out in an argon-filled glovebox. Subsequently, the polymerization reaction was carried out by heating the mixed solution to 180 °C for 12 h under argon. The resulting suspension was cooled to room temperature and filtrated. The filtered solid was washed with NMP and ethanol several times and vacuum-dried at 80 °C. Finally, the polymer material was further washed through Soxhlet extraction in DME for 48 h to remove the soluble short-chain polymer and dried at 80 °C for 12 h under vacuum. The PDI−EDA cathodes were obtained with 50 wt % PDI−DEA powder, 40 wt % ketjen black, and 10 wt % PTFE. These three materials are mixed and molded on a roller press. The loading of the active material was about 3−5 mg $cm^{-2}$.

## ASSOCIATED CONTENT

### Supporting Information

The Supporting Information is available free of charge at https://pubs.acs.org/doi/10.1021/acsnano.4c03968.

> Experimental details including material characterization, electrochemical measurements, MD simulations and DFT calculations method; intrinsic properties of solvents; theoretical calculation results; and additional electrochemical tests (PDF)

## AUTHOR INFORMATION

### Corresponding Author

**Qinyou An** − *State Key Laboratory of Advanced Technology for Materials Synthesis and Processing, Wuhan University of Technology, Wuhan 430070, P. R. China; Hubei Longzhong Laboratory, Wuhan University of Technology (Xiangyang Demonstration Zone), Xiangyang 441000, P. R. China;* orcid.org/0000-0003-0605-4942; Email: anqinyou86@whut.edu.cn

### Authors

**Juncai Long** − *State Key Laboratory of Advanced Technology for Materials Synthesis and Processing, Wuhan University of Technology, Wuhan 430070, P. R. China*

**Yi Liu** − *State Key Laboratory of Advanced Technology for Materials Synthesis and Processing, Wuhan University of Technology, Wuhan 430070, P. R. China*

**Ze He** − *State Key Laboratory of Advanced Technology for Materials Synthesis and Processing, Wuhan University of Technology, Wuhan 430070, P. R. China*

**Shuangshuang Tan** − *College of Materials Science and Engineering, Chongqing University, Chongqing 400044, P. R. China;* orcid.org/0009-0000-4957-1566

**Fangyu Xiong** − *College of Materials Science and Engineering, Chongqing University, Chongqing 400044, P. R. China*

**Hantao Xu** − *State Key Laboratory of Advanced Technology for Materials Synthesis and Processing, Wuhan University of Technology, Wuhan 430070, P. R. China*

**Weixiao Wang** − *State Key Laboratory of Advanced Technology for Materials Synthesis and Processing, Wuhan University of Technology, Wuhan 430070, P. R. China*

**Ge Zhang** − *State Key Laboratory of Advanced Technology for Materials Synthesis and Processing, Wuhan University of Technology, Wuhan 430070, P. R. China*

**Zhongzhuo Yang** − *State Key Laboratory of Advanced Technology for Materials Synthesis and Processing, Wuhan University of Technology, Wuhan 430070, P. R. China*

Complete contact information is available at:
https://pubs.acs.org/10.1021/acsnano.4c03968

### Author Contributions

J.L. and Y.L. contributed equally to this work. The project was supervised by Q.A. All authors discussed the data and commented on the manuscript.

### Notes

The authors declare no competing financial interest.

## ACKNOWLEDGMENTS

This work was supported by the National Key Research and Development Program of China (No. 2023YFB3809501), the National Natural Science Foundation of China (52172231), the Natural Science Foundation of Hubei Province (2022CFA087), and the Fundamental Research Funds for the Central Universities (WUT: 2023-vb-004).

## REFERENCES

(1) Liang, Y.; Dong, H.; Aurbach, D.; Yao, Y. Current status and future directions of multivalent metal-ion batteries. *Nat. Energy* **2020**, *5* (9), 646−656.

(2) Leong, K. W.; Pan, W.; Yi, X.; Luo, S.; Zhao, X.; Zhang, Y.; Wang, Y.; Mao, J.; Chen, Y.; Xuan, J.; et al. Next-generation magnesium-ion batteries: The quasi-solid-state approach to multivalent metal ion storage. *Sci. Adv.* **2023**, *9* (32), No. eadh1181.

(3) Attias, R.; Salama, M.; Hirsch, B.; Goffer, Y.; Aurbach, D. Anode-Electrolyte Interfaces in Secondary Magnesium Batteries. *Joule* **2019**, *3* (1), 27−52.

(4) Kim, H. S.; Arthur, T. S.; Allred, G. D.; Zajicek, J.; Newman, J. G.; Rodnyansky, A. E.; Oliver, A. G.; Boggess, W. C.; Muldoon, J. Structure and compatibility of a magnesium electrolyte with a sulphur cathode. *Nat. Commun.* **2011**, *2*, 427.

(5) Zhang, H.; Qiao, L.; Armand, M. Organic Electrolyte Design for Rechargeable Batteries: From Lithium to Magnesium. *Angew. Chem., Int. Ed.* **2022**, *61*, No. e202214054.

(6) Aurbach, D.; Lu, Z.; Schechter, A.; Gofer, Y.; Gizbar, H.; Turgeman, R.; Cohen, Y.; Moshkovich, M.; Levi, E. Prototype systems for rechargeable magnesium batteries. *Nature* **2000**, *407* (6805), 724−727.

(7) Li, Z.; Häcker, J.; Fichtner, M.; Zhao-Karger, Z. Cathode Materials and Chemistries for Magnesium Batteries: Challenges and Opportunities. *Adv. Energy Mater.* **2023**, *13*, 2300682.

(8) Mohtadi, R.; Tutusaus, O.; Arthur, T. S.; Zhao-Karger, Z.; Fichtner, M. The metamorphosis of rechargeable magnesium batteries. *Joule* **2021**, *5* (3), 581−617.

(9) Lu, Z.; Schechter, A.; Moshkovich, M.; Aurbach, D. On the electrochemical behavior of magnesium electrodes in polar aprotic electrolyte solutions. *J. Electroanal. Chem.* **1999**, *466* (2), 203−217.

(10) Connell, J. G.; Genorio, B.; Lopes, P. P.; Strmcnik, D.; Stamenkovic, V. R.; Markovic, N. M. Tuning the Reversibility of Mg Anodes via Controlled Surface Passivation by $H_2O/Cl^-$ in Organic Electrolytes. *Chem. Mater.* **2016**, *28* (22), 8268−8277.

(11) Mohtadi, R.; Matsui, M.; Arthur, T. S.; Hwang, S. J. Magnesium borohydride: from hydrogen storage to magnesium battery. *Angew. Chem., Int. Ed.* **2012**, *51* (39), 9780−9783.

(12) Tutusaus, O.; Mohtadi, R.; Arthur, T. S.; Mizuno, F.; Nelson, E. G.; Sevryugina, Y. V. An Efficient Halogen-Free Electrolyte for Use in Rechargeable Magnesium Batteries. *Angew. Chem., Int. Ed.* **2015**, *54* (27), 7900−7904.

(13) Zhao-Karger, Z.; Liu, R.; Dai, W.; Li, Z.; Diemant, T.; Vinayan, B. P.; Bonatto Minella, C.; Yu, X.; Manthiram, A.; Behm, R. J.; et al. Toward Highly Reversible Magnesium-Sulfur Batteries with Efficient and Practical Mg[B(hfip)4]2Electrolyte. *ACS Energy Lett.* **2018**, *3* (8), 2005−2013.

(14) Hou, S.; Ji, X.; Gaskell, K.; Wang, P.-f.; Wang, L.; Xu, J.; Sun, R.; Borodin, O.; Wang, C. Solvation sheath reorganization enables divalent metal batteries with fast interfacial charge transfer kinetics. *Science* **2021**, *374* (6564), 172−178.

(15) Zhao, W.; Pan, Z.; Zhang, Y.; Liu, Y.; Dou, H.; Shi, Y.; Zuo, Z.; Zhang, B.; Chen, J.; Zhao, X.; et al. Tailoring Coordination in Conventional Ether-Based Electrolytes for Reversible Magnesium-Metal Anodes. *Angew. Chem., Int. Ed.* **2022**, *61* (30), No. e202205187.

(16) Du, Y.; Chen, Y.; Tan, S.; Chen, J.; Huang, X.; Cui, L.; Long, J.; Wang, Z.; Yao, X.; Shang, B.; et al. Strong solvent coordination effect inducing gradient solid-electrolyte-interphase formation for highly efficient Mg plating/stripping. *Energy Storage Mater.* **2023**, *62*, 102939.

(17) Zhang, D.; Wang, Y.; Yang, Y.; Zhang, Y.; Zhao, Y.; Pan, M.; Sun, Y.; Chen, S.; Liu, X.; Wang, J.; et al. Constructing Efficient Mg(CF3SO3)2 Electrolyte via Tailoring Solvation and Interface Chemistry for High-Performance Rechargeable Magnesium Batteries. *Adv. Energy Mater.* **2023**, *13*, 2301795.

(18) Meng, Y. S.; Srinivasan, V.; Xu, K. Designing better electrolytes. *Science* **2022**, *378* (6624), No. eabq3750.

(19) Wang, F.; Hua, H.; Wu, D.; Li, J.; Xu, Y.; Nie, X.; Zhuang, Y.; Zeng, J.; Zhao, J. Solvent Molecule Design Enables Excellent Charge Transfer Kinetics for a Magnesium Metal Anode. *ACS Energy Lett.* **2023**, *8* (1), 780−789.

(20) Zhang, J.; Liu, J.; Wang, M.; Zhang, Z.; Zhou, Z.; Chen, X.; Du, A.; Dong, S.; Li, Z.; Li, G.; et al. The origin of anode-electrolyte interfacial passivation in rechargeable Mg-metal batteries. *Energy Environ. Sci.* **2023**, *16* (3), 1111−1124.

(21) Zhou, L.; Liu, Q.; Zhang, Z.; Zhang, K.; Xiong, F.; Tan, S.; An, Q.; Kang, Y. M.; Zhou, Z.; Mai, L. Interlayer-Spacing-Regulated VOPO4 Nanosheets with Fast Kinetics for High-Capacity and Durable Rechargeable Magnesium Batteries. *Adv. Mater.* **2018**, *30* (32), 1801984.

(22) Long, J.; Tan, S.; Wang, J.; Xiong, F.; Cui, L.; An, Q.; Mai, L. Revealing the Interfacial Chemistry of Fluoride Alkyl Magnesium Salts in Magnesium Metal Batteries. *Angew. Chem., Int. Ed.* **2023**, *62*, No. e202301934.

(23) Li, Z.; Rao, H.; Atwi, R.; Sivakumar, B. M.; Gwalani, B.; Gray, S.; Han, K. S.; Everett, T. A.; Ajantiwalay, T. A.; Murugesan, V.; et al. Non-polar ether-based electrolyte solutions for stable high-voltage non-aqueous lithium metal batteries. *Nat. Commun.* **2023**, *14* (1), 868.

(24) Salama, M.; Shterenberg, I.; Gizbar, H.; Eliaz, N. N.; Kosa, M.; Keinan-Adamsky, K.; Afri, M.; Shimon, L. J. W.; Gottlieb, H. E.; Major, D. T.; et al. Unique Behavior of Dimethoxyethane (DME)/Mg(N(SO2CF3)2)2 Solutions. *J. Phys. Chem. C* **2016**, *120* (35), 19586−19594.

(25) Wang, D.; Du, X.; Chen, G.; Song, F.; Du, J.; Zhao, J.; Ma, Y.; Wang, J.; Du, A.; Cui, Z.; et al. Cathode Electrolyte Interphase (CEI) Endows $Mo_6$ $S_8$ with Fast Interfacial Magnesium-Ion Transfer Kinetics. *Angew. Chem., Int. Ed.* **2023**, *62* (14), No. e202217709.

(26) Mao, M.; Ji, X.; Wang, Q.; Lin, Z.; Li, M.; Liu, T.; Wang, C.; Hu, Y. S.; Li, H.; Huang, X.; et al. Anion-enrichment interface enables high-voltage anode-free lithium metal batteries. *Nat. Commun.* **2023**, *14* (1), 1082.

(27) Liang, Z.; Ban, C. Strategies to Enable Reversible Magnesium Electrochemistry: From Electrolytes to Artificial Solid-Electrolyte Interphases. *Angew. Chem., Int. Ed.* **2021**, *60* (20), 11036−11047.

(28) Adams, B. D.; Zheng, J.; Ren, X.; Xu, W.; Zhang, J. G. Accurate Determination of Coulombic Efficiency for Lithium Metal Anodes and Lithium Metal Batteries. *Adv. Energy Mater.* **2017**, *8* (7), 1702097.

(29) Chen, X.; Shen, X.; Hou, T.-Z.; Zhang, R.; Peng, H.-J.; Zhang, Q. Ion-Solvent Chemistry-Inspired Cation-Additive Strategy to Stabilize Electrolytes for Sodium-Metal Batteries. *Chem* **2020**, *6* (9), 2242−2256.

(30) Shen, Y.; Wang, Y.; Miao, Y.; Li, Q.; Zhao, X.; Shen, X. Anion-Incorporated Mg-Ion Solvation Modulation Enables Fast Magnesium Storage Kinetics of Conversion-Type Cathode Materials. *Adv. Mater.* **2023**, *35*, 2208289.

(31) Giffin, G. A. The role of concentration in electrolyte solutions for non-aqueous lithium-based batteries. *Nat. Commun.* **2022**, *13* (1), 5250.

(32) Zhao, Y.; Du, A.; Dong, S.; Jiang, F.; Guo, Z.; Ge, X.; Qu, X.; Zhou, X.; Cui, G. A Bismuth-Based Protective Layer for Magnesium Metal Anode in Noncorrosive Electrolytes. *ACS Energy Lett.* **2021**, *6* (7), 2594−2601.

(33) Son, S. B.; Gao, T.; Harvey, S. P.; Steirer, K. X.; Stokes, A.; Norman, A.; Wang, C.; Cresce, A.; Xu, K.; Ban, C. An artificial interphase enables reversible magnesium chemistry in carbonate electrolytes. *Nat. Chem.* **2018**, *10* (5), 532−539.

(34) Dedryvère, R.; Leroy, S.; Martinez, H.; Blanchard, F.; Lemordant, D.; Gonbeau, D. XPS Valence Characterization of Lithium Salts as a Tool to Study Electrode/Electrolyte Interfaces of Li-Ion Batteries. *J. Phys. Chem. B* **2006**, *110* (26), 12986−12992.

(35) Horia, R.; Nguyen, D. T.; Eng, A. Y. S.; Seh, Z. W. Using a Chloride-Free Magnesium Battery Electrolyte to Form a Robust Anode-Electrolyte Nanointerface. *Nano Lett.* **2021**, *21* (19), 8220−8228.

(36) Li, P.; Sun, Z.-T.; Wang, Y.; Razaq, R.; Gao, Y.; Bo, S.-H. Overpotential-Regulated Stable Cycling of a Thin Magnesium Metal Anode. *ACS Appl. Mater. Interfaces* **2022**, *14* (27), 31435−31447.

(37) Liu, X.; Du, A.; Guo, Z.; Wang, C.; Zhou, X.; Zhao, J.; Sun, F.; Dong, S.; Cui, G. Uneven Stripping Behavior, an Unheeded Killer of Mg Anodes. *Adv. Mater.* **2022**, *34*, 2201886.

(38) Dong, H.; Liang, Y.; Tutusaus, O.; Mohtadi, R.; Zhang, Y.; Hao, F.; Yao, Y. Directing Mg-Storage Chemistry in Organic Polymers toward High-Energy Mg Batteries. *Joule* **2019**, *3* (3), 782−793.

(39) Li, C.; Shyamsunder, A.; Key, B.; Yu, Z.; Nazar, L. F. Stabilizing magnesium plating by a low-cost inorganic surface membrane for high-voltage and high-power Mg batteries. *Joule* **2023**, *7*, 2798−2813.

(40) Yang, G.; Li, Y.; Wang, J.; Lum, Y.; Lim, C. Y. J.; Ng, M.-F.; Zhang, C.; Chang, Z.; Zhang, Z.; Handoko, A. D.; et al. Realizing horizontal magnesium platelet deposition and suppressed surface passivation for high-performance magnesium metal batteries. *Energy Environ. Sci.* **2024**, *17*, 1141−1152.

(41) Li, Z.; Mu, X.; Zhao-Karger, Z.; Diemant, T.; Behm, R. J.; Kubel, C.; Fichtner, M. Fast kinetics of multivalent intercalation chemistry enabled by solvated magnesium-ions into self-established metallic layered materials. *Nat. Commun.* **2018**, *9* (1), 5115.

(42) Ren, W.; Wu, D.; NuLi, Y.; Zhang, D.; Yang, Y.; Wang, Y.; Yang, J.; Wang, J. An Efficient Bulky Mg[B(Otfe)4]2 Electrolyte and Its Derivatively General Design Strategy for Rechargeable Magnesium Batteries. *ACS Energy Lett.* **2021**, *6* (9), 3212−3220.

(43) Herb, J. T.; Nist-Lund, C. A.; Arnold, C. B. A Fluorinated Alkoxyaluminate Electrolyte for Magnesium-Ion Batteries. *ACS Energy Lett.* **2016**, *1* (6), 1227−1232.

(44) Mizrahi, O.; Amir, N.; Pollak, E.; Chusid, O.; Marks, V.; Gottlieb, H.; Larush, L.; Zinigrad, E.; Aurbach, D. Electrolyte Solutions with a Wide Electrochemical Window for Rechargeable Magnesium Batteries. *J. Electrochem. Soc.* **2008**, *155* (2), A103.

(45) Lancry, E.; Levi, E.; Mitelman, A.; Malovany, S.; Aurbach, D. Molten salt synthesis (MSS) of $Cu_2Mo_6S_8$—New way for large-scale production of Chevrel phases. *J. Solid State Chem.* **2006**, *179* (6), 1879−1882.

(46) Lu, D.; Liu, H.; Huang, T.; Xu, Z.; Ma, L.; Yang, P.; Qiang, P.; Zhang, F.; Wu, D. Magnesium ion based organic secondary batteries. *J. Mater. Chem. A* **2018**, *6* (36), 17297−17302.